Theoretical modeling of tunable vibrations of three-dimensional serpentine structures for simultaneous measurement of adherent cell mass and modulus

Jianzhong Zhao†, Weican Li†, Xingming Guo, Heling Wang*, John A. Rogers, and Yonggang Huang

Submitted April 19, 2020; Accepted August 24, 2020

Vibration-based methods can be used effectively to characterize the physical properties of biological materials, with an increasing interest focused on the mechanics of individual, living cells. Real-time measurements of cell properties, such as mass and Young's modulus, can yield important insights into many aspects of cell growth and metabolism as well as the interaction of cells with external stimuli (e.g., drugs). Vibrational test structures designed for the study of such cell properties often use fixed configurations and operational modes, with associated limitations in determining multiple characteristics of the cell, simultaneously. Recent development of mechanics-guided techniques for deterministic assembly of three-dimensional (3D) microstructures provides a route to vibrational frameworks that offer tunable configurations, vibration modes, and resonant frequencies. Here we propose a method that exploits such tunable vibrational structures to simultaneously determine the mass and modulus of a single adherent cell, or of other biological materials or small-scale living systems (e.g., organoids), through theoretical modeling and finite element analysis. The idea involves a 3D architecture that supports two different vibrational structures and can be converted from one to the other through application of strain to an elastomeric substrate. Specifically, tailored designs for serpentine ribbons in these systems enable a decoupling of the dependence of the resonant frequencies of the two structures to the cell mass and modulus, with an associated ability to measure these two properties accurately and independently. These same concepts can be scaled to apply to various types of cells, as well as to organoids (3D clusters of cells) and other biological materials with small geometries, across a range of values of mass and modulus. This method could serve as the foundation for microelectromechanical systems capable of monitoring mass and modulus in real time for use in research in biomechanics and dynamic biological processes.

Cell mass and modulus are important indicators of cell behavior during growth, proliferation, differentiation, and interactions with external stimuli such as drugs and viruses. We propose a method to simultaneously measure cell mass and modulus through the use of the vibrations of tunable three-dimensional (3D) structures formed via a mechanics-guided assembly approach. The method is applicable to various types of cells and other biological materials and small-scale living systems across a wide range of values of mass and modulus. The results may serve as the foundation for microelectromechanical systems capable of monitoring physical aspects of cellular processes in real time.

Introduction

Vibrational structures with submillimeter dimensions have been widely adopted in determining the physical properties of materials such as cells,[1–12] blood,[13,14] and nanofibers/nanowires.[15–18] Vibration-based methods in cell mechanics is of growing interest because of their rapid and non-invasive ability to monitor cellular processes in real time.[1–6,9,19–22] For example, a micrometer-scale cantilever actuated by a beam of laser light enables the continuous (millisecond time resolution) measurement of cell mass with high resolution (picogram) from the shift of its resonant frequency.[3] However, these and other related vibrational

Jianzhong Zhao, Shanghai Institute of Applied Mathematics and Mechanics, Shanghai Key Laboratory of Mechanics in Energy Engineering, School of Mechanics and Engineering Science, Shanghai University, People's Republic of China; Departments of Civil and Environmental Engineering, Mechanical Engineering, and Materials Science and Engineering, Northwestern University, Illinois, USA
Weican Li, School of Engineering, Brown University, Rhode Island, USA
Xingming Guo, Shanghai Institute of Applied Mathematics and Mechanics, Shanghai Key Laboratory of Mechanics in Energy Engineering, School of Mechanics and Engineering Science, Shanghai University, People's Republic of China
Heling Wang, Departments of Civil and Environmental Engineering, Mechanical Engineering, and Materials Science and Engineering, Northwestern University, Illinois, USA
John A. Rogers, Departments of Materials Science and Engineering, Biomedical Engineering, Chemistry, Mechanical Engineering, Electrical Engineering and Computer Science, and Neurological Surgery, Northwestern University, Illinois, USA; Querrey-Simpson Institute for Bioelectronics, Northwestern University, Illinois, USA
Yonggang Huang, Departments of Civil and Environmental Engineering, Mechanical Engineering, and Materials Science and Engineering, Northwestern University, Illinois, USA; Querrey-Simpson Institute for Bioelectronics, Northwestern University, Illinois, USA
*Corresponding author. Email: helingwang1@gmail.com
†These authors contributed equally to this work.
doi:10.1557/s43577-021-00043-1

structures focus mainly on the measurement of a single property of the cell, such as mass. For many envisioned uses, multi-parameter monitoring (e.g., mass and Young's modulus) during cell growth or interactions with the surrounding environment (e.g., drugs and virus) can be important. Vibrational structures with fixed architectures and operational modes cannot, in most cases, be used for simultaneous determination of multiple cell properties, as the inverse problem involves multiple, coupled unknowns. A microelectromechanical system (MEMS) sensor reported by Park et al.[2] measures cell mass, modulus, and viscosity simultaneously, but it requires at least four cells with different masses and a fixation procedure to alter the cell modulus and viscosity. The multimode nanomechanical resonators reported by Malvar et al.[23] measure the mass and modulus of nanoparticle and bacteria simultaneously, but the sample modulus is on the order of GPa, which is about 3~6 orders of amplitude larger than that of soft, biological materials.[3,24,25] Kang et al.[26] determined the mass and modulus of suspension cells simultaneously, but the reported fractional shift in the resonant frequency is on the order of only 10^{-6}, which requires a very accurate measurement of the resonant frequency.

One major difficulty associated with vibrational methods in measuring multiple cell properties simultaneously is that the number of outputs (e.g., shifts of resonant frequencies) is limited, as the shape and the operational mode of the vibrational structure are fixed. Recent advances in techniques for mechanics-guided, deterministic assembly of three-dimensional (3D) mesostructures provide routes to morphable 3D systems with complex architectures and in geometries that can be dynamically selected in a systematic way.[27–35] Such 3D vibrational structures form via processes of guided buckling of a corresponding 2D precursor because of compressive forces imparted onto them with a prestrained elastomeric substrate. Such substrates can be stretched or compressed after this assembly process to tune the shapes in a systematic, reversible, and well-controlled manner.[36–38] In particular, the natural frequency and vibration mode of a 3D structure are significantly different from those of the 2D precursor (flat structure).[36,37,39,40] Diverse functional materials, such as piezoelectric membranes,[41] thin metal films,[42–45] doped silicon nanostructures,[46,47] shape memory polymers,[29,48,49] and elastomers[50,51] can be easily integrated into these dynamic 3D structures, thus providing the basis for multiple options in actuation and sensing.

Here we propose a method that uses two 3D vibrational structures with distinguishable vibration modes and natural frequencies to measure the adherent cell mass and modulus simultaneously. The two structures are formed via the mechanics-guided, deterministic 3D assembly technique from the same 2D precursor and can be induced to switch from one to the other via strains applied to the substrate. A key feature is that the functional parts of the structures adopt serpentine shapes.[52,53] Compared to conventional 3D structures formed via buckling, such serpentine structures offer low stiffnesses[52,53] comparable to those of cells, thereby favoring the measurement of the cell modulus. Via tailored selection of the geometrical parameters of the serpentine structures, the approach can be optimized to apply to several types of cells such as osteoblasts, fibroblasts, and HeLa cells (with mass typically from 2 ng to 14 ng and modulus from 2 kPa to 20 kPa[3,24,54]). Using general scaling laws from an analysis of the underlying mechanics, these designs can be scaled to apply to additional types of cells with various values of mass and modulus, as well as to other small-scale biological systems such as organoids.

Approach and formulation

The tunable 3D structures and their vibration

A schematic illustration of the tunable 3D structures is shown in **Figure 1**, where the serpentine ribbon is the vibrational part. A small disk introduced at the center of the structure serves as a support for a cell. The 2D precursor (Figure 1a) is selectively bonded to a substrate with prestrains (ε_{Prex} and ε_{Prey}) in both *x*- and *y*-directions. Structure 1 forms from release of the prestrain only in the *x*-direction, such that the serpentine ribbon remains flat; Structure 2 forms by subsequently releasing the prestrain in the *y*-direction, and the serpentine ribbon buckles up (Figure 1b). The two structures are formed from the same 2D precursor and can switch from one to the other via the substrate strain. The vibrations of both structures can be actuated by a vibrational stage attached to the bottom of the substrate[36] or by a Lorentz force setup.[2] This study adopts a vibrational stage that moves vertically in a periodic manner to actuate the out-of-plane vibration mode (Figure 1c). A laser system can measure the resonant frequency by a laser system.[2,36,41,55]

Resonant frequency of the serpentine ribbon without the cell

The stiffness of the serpentine ribbon is much smaller than the supportive straight ribbon,[52] such that in the first-order out-of-plane vibration mode, only the serpentine ribbon vibrates (see Figure 1c), and the resonant frequency is independent of the straight ribbon and the substrate.[37] Our prior work[52] demonstrated that the resonant frequency (first-order out-of-plane mode, small deformation) of the serpentine ribbon obeys the following scaling law

$$f_{Struc} = \alpha(\varepsilon)\sqrt{\frac{E_{Struc}}{\rho_{Struc}}}\frac{h_{Struc}}{HS}, \quad (1)$$

where E_{Struc}, ρ_{Struc}, H, S, and h_{Struc} stand for the serpentine modulus, mass density, height, total arc length and cross-sectional thickness, respectively (see Figure 1a), and the coefficient $\alpha(\varepsilon)$ depends on the compressive strain $\varepsilon = \varepsilon_{Prey}/(1+\varepsilon_{Prey})$ applied on the serpentine ribbon ($\varepsilon = 0$ for Structure 1 and $\varepsilon \sim 10\%$ for Structure 2). The scaling law holds for $L \ll S$ and $h_{Struc} \ll b_{Struc}$ (L, serpentine length; b_{Struc}, cross-sectional width; see Figure S1 for finite element analysis (FEA) demonstration and **Appendix A** for details of the FEA). For a representative compressive strain $\varepsilon = 10\%$, the resonant frequency

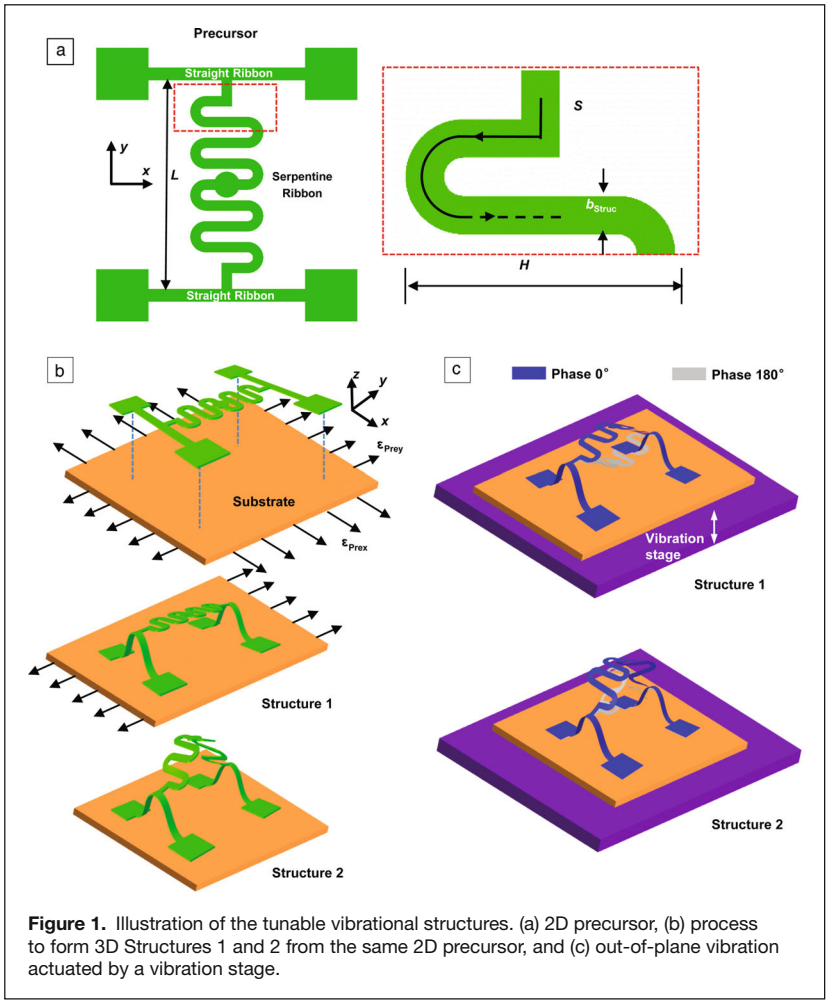

Figure 1. Illustration of the tunable vibrational structures. (a) 2D precursor, (b) process to form 3D Structures 1 and 2 from the same 2D precursor, and (c) out-of-plane vibration actuated by a vibration stage.

f_{Struc2} of the buckled serpentine ribbon (Structure 2) is larger than the resonant frequency f_{Struc1} of the flat serpentine ribbon (Structure 1, see Figure S1). Even though the scaling law in Equation 1 does not account for the small disk at the center of the structure, it is useful for purposes of selecting the design for the resonant frequency of the tunable serpentine structures.

Resonant frequency of the cell on a rigid base

The cell shape (and some other biological materials such as organoids), which can be measured by standard optical methods,[2,9] is often modeled as a spherical cap (as shown in **Figure 2** and Figure S2) in prior studies,[2,9,56] where h_{Cell}/a_{Cell} reflects the cell shape (h_{Cell} and a_{Cell}—spherical cap height and radius, respectively, see Figure S2). For cells with their bottoms fixed on a rigid base, dimensional analysis yields the following scaling law for the resonant frequency (small deformation, see Figure S2 for FEA demonstration)

$$f_{Cell} = \left(\frac{E_{Cell}^3}{m_{Cell}^2 \rho_{Cell}}\right)^{\frac{1}{6}} C\left(\frac{h_{Cell}}{a_{Cell}}\right), \quad (2)$$

where m_{Cell}, E_{Cell}, and ρ_{Cell} correspond to cell mass, modulus, and mass density, respectively, and the function C to be determined depends on the cell shape. Depending on the types of cell, the human cell mass ranges from 0.1 ng (neutrophil) to 1000 ng (ovum), and modulus ranges from 0.1 kPa (lymphocyte) to 100 kPa (cardiomyocyte).[3,24,25] The wide range of cell properties makes it difficult for a single design to apply effectively to all types of cells. The design of the tunable structures presented in the next section aims at osteoblasts, fibroblasts, and HeLa cells (2 ng < m_{Cell} < 14 ng and 2 < E_{Cell} < 20 kPa), which are the cells that produce bones, secrete collagen proteins, and are widely used in cancer research, respectively. Based on the scaling laws in Equations 1 and 2, these designs can be scaled to apply to other types of cells or other soft materials (see the section on "Scale the design for other types of cell or biological materials").

Vibration of the structures with cells

Placing a cell on the central disk of the serpentine structure yields a combined 3D structure–cell system with a resonant frequency f that depends on the properties of both the serpentine ribbon and the cell (see Figure 2). Determining the cell mass and modulus from one output (resonant frequency) of a single structure is difficult. The proposed tunable structures, which correspond to two distinct structures formed from the same 2D precursor, provide two outputs (i.e., two resonant frequencies $f_{Struc1\text{-}Cell}$ and $f_{Struc2\text{-}Cell}$) to facilitate determination of the cell mass and modulus simultaneously,

$$\begin{cases} f_{Struc1\text{-}Cell} = F_1(m_{Cell}, E_{Cell}) \\ f_{Struc2\text{-}Cell} = F_2(m_{Cell}, E_{Cell}) \end{cases}. \quad (3)$$

In addition, for a tailored design of the serpentine ribbon with E_{Struc} = 4.02 GPa[34] and ρ_{Struc} = 1220 kg/m^3 [36] for polyimide and H = 90 μm, S = 1000 μm, h_{Struc} = 4 μm, and b_{Struc} = 20 μm, Equation 3 becomes approximately decoupled, especially for the range of cell mass 6 ng < m_{Cell} < 14 ng and modulus 4 kPa < E_{Cell} < 10 kPa.

Structure 1 (flat serpentine) is designed to have its resonant frequency f_{Struc1} (~19.2 kHz) close to $f_{Struc1\text{-}Cell}$ (~17–18 kHz, see Figure 2b) of the structure–cell system, but both are much smaller than f_{Cell} (~33.6–70.5 kHz for h_{Cell}/a_{Cell} = 0.5[2]) of the cell, such that the cell does not deform significantly near the

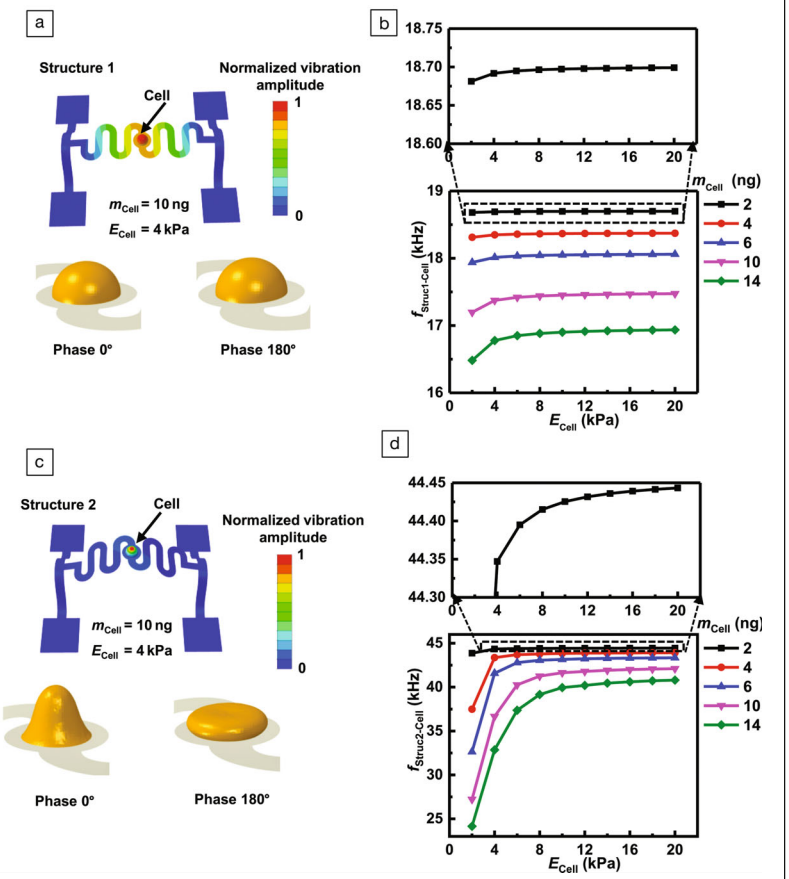

Figure 2. Vibration of the structure with cells. (a, c) Vibration amplitude of Structures 1 and 2 with cells, respectively. (b, d) Relationship of the resonant frequency versus cell mass and modulus, for Structures 1 and 2, respectively. The cell shape is $h_{Cell}/a_{Cell} = 0.5$. The vibration amplitudes in the images of (a) and (c) show the cell deformation. The actual deformations of both the cell and the structure are in the linear elastic range (small deformation).

resonant frequency $f_{Struc1\text{-}Cell}$ of the structure–cell system (see Figure 2a for the vibration amplitude). Therefore, the resonant frequency $f_{Struc1\text{-}Cell}$ is insensitive to the cell modulus, as shown in Figure 2b (for 6 ng < m_{Cell} < 14 ng and 4 kPa < E_{Cell} < 10 kPa). Meanwhile, the mass of Structure 1 is designed to be comparable to the cell mass m_{Cell} such that the resonant frequency $f_{Struc1\text{-}Cell}$ depends on m_{Cell} (Figure 2b), from which m_{Cell} can be determined,

$$f_{Struc1\text{-}Cell} = F_1(m_{Cell}, E_{Cell}) \approx F_1(m_{Cell}). \quad (4)$$

The resonant frequency f_{Struc2} (~44.9 kHz) of Structure 2 (buckled serpentine ribbon) is much larger than f_{Struc1} (~19.2 kHz) of Structure 1, and is close to f_{Cell} (~33.6–70.5 kHz) of the cell, such that $f_{Struc2\text{-}Cell}$ (~25–45 kHz, see Figure 2d) of the structure–cell system is also close to f_{Cell}. Therefore, the cell deforms significantly as compared to that in Structure 1 (but still in the linear elastic regime) at the resonant frequency $f_{Struc2\text{-}Cell}$ (see Figure 2c) such that the cell modulus E_{Cell} is an important parameter (Figure 2d), which can then be determined from the second equation in Equation 3.

For an expanded range of cell properties (e.g., 2 ng < m_{cell} < 14 ng and 2 kPa < E_{cell} < 20 kPa), the two equations for cell mass and modulus in Equation 3 are coupled, but they can still be solved numerically.

The accuracy in the measured resonant frequency is estimated to be ~1 Hz, according to the report by Park et al.[2] for the resonant frequency on the order of 10–100 kHz using laser Doppler vibrometer. As shown in **Appendix B**, the proposed approach predicts the maximum uncertainty of 0.42% for the cell mass and 5.2% for the cell modulus, for the range 2 ng < m_{Cell} < 14 ng and 2 kPa < E_{Cell} < 20 kPa. These maximum uncertainties are reached only within a small range of cell mass, m_{Cell} < 6ng. Beyond this range (i.e., 6 ng ≤ m_{Cell} ≤ 14 ng and 2 kPa ≤ E_{Cell} ≤ 20 kPa), the uncertainty is much less, only 0.12% for cell mass and 0.89% for cell modulus.

Scale the design for other types of cell or biological materials

Based on the scaling laws and the design strategy in the previous section, the serpentine ribbon can be scaled to measure simultaneously the mass and modulus of other types of cells or biological materials. For example, organoids, which are composed of several hundred cells, have drawn increasing research interest recently.[56–59] For representative organoids, where the mass is 200 ng < m_{Orga} < 1000 ng (~100 times of the single cell mass studied in the previous section) and the modulus is 0.5 kPa < E_{Orga} < 5 kPa, the resonant frequency is 2.9 kHz < f_{Orga} < 14.5 kHz, much smaller than that of cells in the previous section. Therefore, the resonant frequency of the serpentine ribbon should also decrease and provide a mass comparable to that of the organoid. These characteristics are not difficult to achieve, such as with H = 300 μm, S = 8000 μm, h_{Struc} = 9 μm and b_{Struc} = 50 μm, and E_{Struc} = 4.02 GPa[34] and ρ_{Struc} = 1220 kg/m^3 [36] for polyimide, as shown in **Figure 3**. The estimated error is 0.41% for mass and 3.4% error for modulus.

Another example focuses on cells or biological materials with very small mass and modulus (e.g., 0.1 ng < m_{cell} < 1 ng and 0.1 kPa < E_{cell} < 0.5 kPa), which are close to the lower bounds for the properties of human cells. With H = 75 μm,

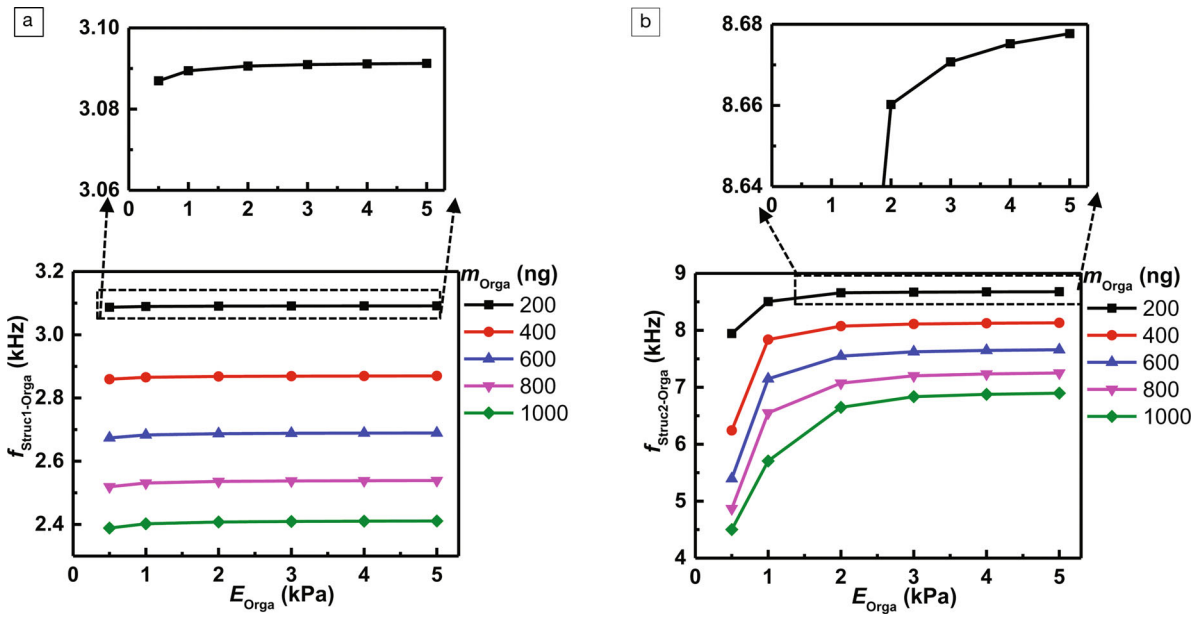

Figure 3. Vibration of the structure with organoids. Relationship of the resonant frequency versus organoids mass and modulus, for (a) Structure 1 and (b) Structure 2. The organoids are modeled as a spherical cap with $h_{Orga}/a_{Orga} = 0.5$.

$S = 950\,\mu m$, $h_{Struc} = 1\,\mu m$ and $b_{Struc} = 5\,\mu m$, and $E_{Struc} = 4.02$ GPa[34] and $\rho_{Struc} = 1220\,kg/m^3$ [36] for polyimide, the proposed method can determine m_{cell} and E_{cell} in this range with an estimated error of 0.54% for mass and 7.0% error for modulus (see Figure S3 for the relationships of resonant frequencies versus cell mass and modulus), again assuming ideal behaviors as captured by these modeling approaches. This feasibility in scaling the design arises from the rich design options of the serpentine ribbon.

Discussions

Effect of fluid

Living cells are usually immersed in fluids in their physiological environment. With the inertia of the fluids (density $1\,g/cm^3$, close to the physiological environment of cells) taken into consideration via the acoustic–structure interaction,[26] the simulations illustrate that the relationships of the resonant frequencies of the two structures versus cell properties show a similar trend as that presented previously. As shown in **Figure 4**, in the range $6\,ng < m_{Cell} < 14\,ng$ and $2\,kPa < E_{Cell} < 14\,kPa$, the resonant frequency of Structure 1 (flat serpentine) is approximately insensitive to the cell modulus, whereas that of Structure 2 (buckled serpentine) is sensitive to the cell modulus. This range of cell properties is narrower than that presented previously, because the added mass of the fluid decreases the resonant frequency of the structure–cell system, and therefore decreases the sensitivity. However, this range still overlaps with the mass and modulus of a few biological materials.[60–62] The design of serpentines can also be scaled to work for other ranges of cell properties. This study demonstrates that the proposed method may still work when the cells are immersed in their physiological environments.

Effect of frequency-dependent modulus

As reported by Rigato et al., the cell modulus may change with the frequency.[63] Considering this frequency-dependent modulus, the proposed method may still determine the cell modulus around the resonant frequency of Structure 2. For the serpentine structure presented previously, when the cell mass (m_{Cell}) and modulus (E_{Cell}) are in the range $6\,ng < m_{Cell} < 14\,ng$ and $4\,kPa < E_{Cell} < 10\,kPa$, respectively, Structure 1 can determine the cell mass without involving the modulus. Given the cell mass, determining the cell modulus only requires the resonant frequency of Structure 2, which does not span a very large range (32.85 kHz–40.80 kHz). Based on the experiment and the double power law in Rigato et al.,[63] the relative change of the cell modulus with frequency is no more than 10% in the previous frequency range. Therefore, it is reasonable to assume a frequency-independent cell modulus in our method when the cell properties are limited. The design of the serpentine structures can be scaled such that this concept is valid for other ranges of cell properties.

Conclusions

Two serpentine structures formed from the same 2D precursor via mechanics-guided, deterministic, 3D assembly provide a straightforward means to measure the mass and modulus of a single adherent cell, simultaneously. The key concept is that the resonant frequency of Structure 1 is

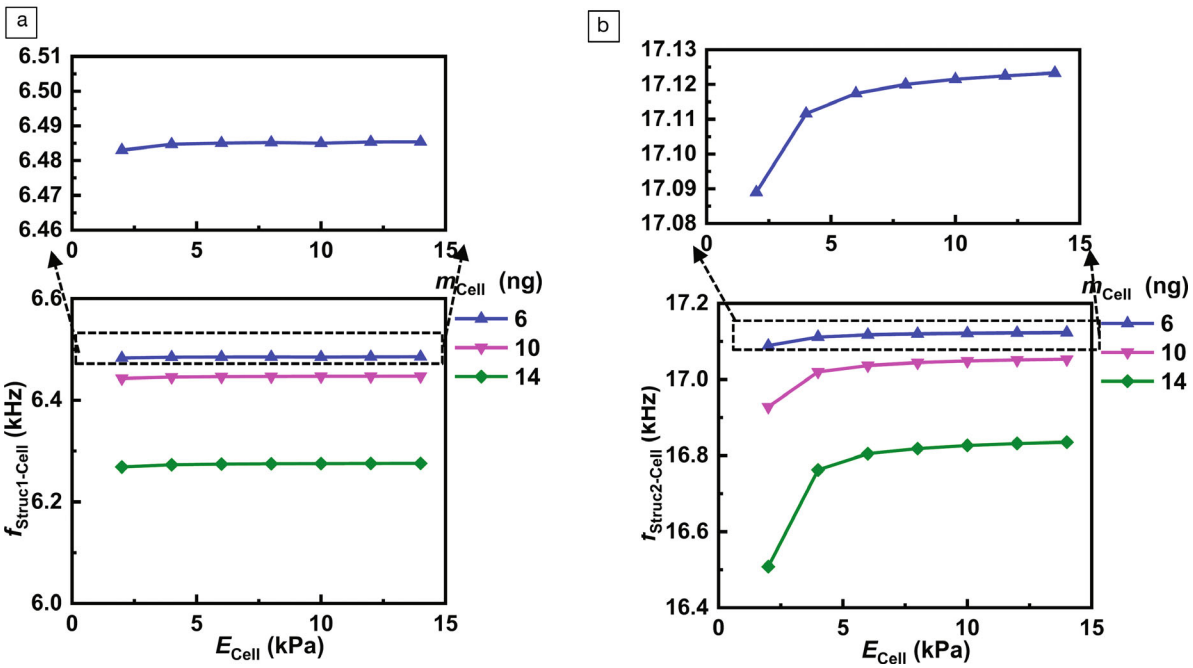

Figure 4. Vibration of the structure with cells emerged in fluids. Relationship of the resonant frequency versus cell mass and modulus for (a) Structure 1 and (b) Structure 2. The cell shape is $h_{Cell}/a_{Cell} = 0.5$.

designed to be much smaller than that of the cell, while that of Structure 2 is close to that of the cell. The rich design options supported by serpentine ribbons in these structures allow the approach to be scaled to operate effectively for various types of cells and other biological materials with mass and modulus across a wide range. The proposed approach may serve as the basis of MEMS to monitor the cell mass and modulus in real time.

Supplementary material

To view supplementary material for this article, please visit https://doi.org/10.1557/s43577-021-00043-1.

Acknowledgments

J.Z. acknowledges the support from the China Scholarship Council. The authors appreciate Prof. Xin Ning from Pennsylvania State University and Prof. Yihui Zhang from Tsinghua University for useful discussions.

Appendices

A. Finite element analysis

The simulation for the compressive buckling and vibration of 3D structures followed the same approach as in prior studies,[36,52] performed by the commercial software ABAQUS. The vibrational structure is modeled by four-node shell elements. The cell and organoids are modeled by eight-node solid elements. The cell and the organoids are perfectly bonded to the vibrational structure by tie constraint.

B. Accuracy analysis

For the measurement of cell properties in the sections on "Vibrations of the structures with cells" and "Scale the design for other types of cell or biological materials," given the resonant frequencies $f_{Struc1-Cell}$ and $f_{Struc2-Cell}$, the cell mass m_{Cell} and modulus E_{Cell} can be solved numerically from Equation 3. Then for $f_{Struc1-Cell} \pm 1$ Hz and $f_{Struc2-Cell} \pm 1$ Hz, Equation 3 is solved again, and the differences in the solutions give the errors.

References

1. E.A. Corbin, F. Kong, C.T. Lim, W.P. King, R. Bashir, Biophysical properties of human breast cancer cells measured using silicon MEMS resonators and atomic force microscopy. *Lab on a Chip* **15**, 839 (2015).
2. K. Park, L.J. Millet, N. Kim, H. Li, X. Jin, G. Popescu, N.R. Aluru, K.J. Hsia, R. Bashir, Measurement of adherent cell mass and growth. *Proc. Natl. Acad. Sci. U.S.A.* **107**, 20691 (2010).
3. D. Martinez-Martin, G. Flaschner, B. Gaub, S. Martin, R. Newton, C. Beerli, J. Mercer, C. Gerber, D.J. Muller, Inertial picobalance reveals fast mass fluctuations in mammalian cells. *Nature* **550**, 500 (2017).
4. M. Shaat, A. Abdelkefi, Modeling the material structure and couple stress effects of nanocrystalline silicon beams for pull-in and bio-mass sensing applications. *Int. J. Mech. Sci.* **101**, 280 (2015).
5. K. Park, J. Jang, D. Irimia, J. Sturgis, J. Lee, J.P. Robinson, M. Toner, R. Bashir, 'Living cantilever arrays' for characterization of mass of single live cells in fluids. *Lab on a Chip* **8**, 1034 (2008).
6. A.K. Bryan, V.C. Hecht, W. Shen, K. Payer, W.H. Grover, S.R. Manalis, Measuring single cell mass, volume, and density with dual suspended microchannel resonators. *Lab on a Chip* **14**, 569 (2014).
7. M.H. Rahman, M.R. Ahmad, M. Takeuchi, M. Nakajima, Y. Hasegawa, T. Fukuda, Single cell mass measurement using drag force inside lab-on-chip microfluidics system. *IEEE transactions on nanobioscience* **14**, 927 (2015).
8. N. Cermak, S. Olcum, F.F. Delgado, S.C. Wasserman, K.R. Payer, M.A. Murakami, S.M. Knudsen, R.J. Kimmerling, M.M. Stevens, Y. Kikuchi, A. Sandikci, M. Ogawa, V. Agache, F. Baléras, D.M. Weinstock, S.R. Manalis,

High-throughput measurement of single-cell growth rates using serial microfluidic mass sensor arrays. *Nat. Biotechnol.* **34**, 1052 (2016).
9. E.A. Corbin, O.O. Adeniba, R.H. Ewoldt, R. Bashir, Dynamic mechanical measurement of the viscoelasticity of single adherent cells. *Appl. Phys. Lett.* **108**, 093701 (2016).
10. Y. Kurashina, M. Hirano, C. Imashiro, K. Totani, J. Komotori, K. Takemura, Enzyme-free cell detachment mediated by resonance vibration with temperature modulation. *Biotechnol. Bioeng.* **114**, 2279 (2017).
11. Y. Kurashina, K. Takemura, J. Friend, S. Miyata, J. Komotori, Efficient subculture process for adherent cells by selective collection using cultivation substrate vibration. *IEEE Transactions on Biomedical Engineering* **64**, 580 (2016).
12. A. Bouchaala, A.H. Nayfeh, M.I. Younis, Frequency shifts of micro and nano cantilever beam resonators due to added masses. *J. Dyn. Sys., Meas., Control* **138**, 091002 (2016).
13. H. Lin, M. Chung, L. Huang, An oscillated, self-sensing piezoresistive microcantilever sensor with fast fourier transform analysis for point-of-care blood coagulation monitoring. *2016 IEEE International Conference on Industrial Technology*, 640 (2016).
14. X. Lu, L. Hou, L. Zhang, Y. Tong, G. Zhao, Z.Y. Cheng, Piezoelectric-excited membrane for liquids viscosity and mass density measurement. *Sensor. Actuat. A-Phys.* **261**, 196 (2017).
15. E. Gil-Santos, D. Ramos, J. Martínez, M. Fernández-Regúlez, R. García, Á.S. Paulo, M. Calleja, J. Tamayo, Nanomechanical mass sensing and stiffness spectrometry based on two-dimensional vibrations of resonant nanowires. *Nat. Nanotechnol.* **5**, 641 (2010).
16. M. Li, H.X. Tang, M.L. Roukes, Ultra-sensitive NEMS-based cantilevers for sensing, scanned probe and very high-frequency applications. *Nat. Nanotechnol.* **2**, 114 (2007).
17. Y.T. Yang, C. Callegari, X.L. Feng, K.L. Ekinci, M.L. Roukes, Zeptogram-scale nanomechanical mass sensing. *Nano Letters* **6**, 583 (2006).
18. K. Jensen, K. Kim, A. Zettl, An atomic-resolution nanomechanical mass sensor. *Nat. Nanotechnol.* **3**, 533 (2008).
19. N. Cermak, S. Olcum, F.F. Delgado, S.C. Wasserman, K.R. Payer, M.A. Murakami, S.M. Knudsen, R.J. Kimmerling, M.M. Stevens, Y. Kikuchi, A. Sandikci, M. Ogawa, V. Agache, F. Baléras, D.M. Weinstock, S.R. Manalis, High-throughput measurement of single-cell growth rates using serial microfluidic mass sensor arrays. *Nat. Biotechnol* **34**, 1052 (2016).
20. E. Sage, M. Sansa, S. Fostner, M. Defoort, M. Gély, A.K. Naik, R. Morel, L. Duraffourg, M.L. Roukes, T. Alava, G. Jourdan, E. Colinet, C. Masselon, A. Brenac, S. Hentz, Single-particle mass spectrometry with arrays of frequency-addressed nanomechanical resonators. *Nat. Commun.* **9**, 3283 (2018).
21. A. Martín-Perez, D. Ramos, E. Gil-Santos, S. García-Lopez, M.L. Yubero, P.M. Kosaka, A.S. Paulo, J. Tamayo, M. Calleja, Mechano-optical analysis of single cells with transparent microcapillary resonators. *ACS Sensors* **4**, 3325 (2019).
22. D.P. Annalisa, L.G. Villanueva, Suspended micro/nano channel resonators: a review. *J. Micromech. Microeng* **30**, 4 (2020).
23. O. Malvar, J.J. Ruz, P.M. Kosaka, C.M. Domínguez, E. Gil-Santos, M. Calleja, J. Tamayo, Mass and stiffness spectrometry of nanoparticles and whole intact bacteria by multimode nanomechanical resonators. *Nat. Commun.* **7**, 13452 (2016).
24. R. Narayan, *Encyclopedia of Biomedical Engineering* (Elsevier, New York, 2018).
25. G. Lin, X. Zhang, J. Ren, Z. Pang, C. Wang, N. Xu, R. Xi, Integrin signaling is required for maintenance and proliferation of intestinal stem cells in Drosophila. *Developmental Biology* **377**, 177 (2013).
26 J.H. Kang, T.P. Miettinen, L. Chen, S. Olcum, G. Katsikis, P.S. Doyle, S.R. Manalis, Noninvasive monitoring of single-cell mechanics by acoustic scattering. *Nat. Methods* **16**, 3 (2019).
27. H. Fu, K. Nan, W. Bai, W. Huang, K. Bai, L. Lu, C. Zhou, Y. Liu, F. Liu, J. Wang, M. Han, Z. Yan, H. Luan, Y. Zhang, Y. Zhang, J. Zhao, X. Cheng, M. Li, J.W. Lee, Y. Liu, D. Fang, X. Li, Y. Huang, Y. Zhang, J.A. Rogers, Morphable 3D mesostructures and microelectronic devices by multistable buckling mechanics. *Nat. Mater.* **17**, 268 (2018).
28. Z. Yan, F. Zhang, F. Liu, M. Han, D. Ou, Y. Liu, Q. Lin, X. Guo, H. Fu, Z. Xie, M. Gao, Y. Huang, J. Kim, Y. Qiu, K. Nan, J. Kim, P. Gutruf, H. Luo, A. Zhao, K. Hwang, Y. Huang, Y. Zhang, J.A. Rogers, Mechanical assembly of complex, 3D mesostructures from releasable multilayers of advanced materials. *Sci. Adv.* **2**, e1601014 (2016).
29. X. Wang, X. Guo, J. Ye, N. Zheng, P. Kohli, D. Choi, Y. Zhang, Z. Xie, Q. Zhang, H. Luan, K. Nan, B.H. Kim, Y. Xu, X. Shan, W. Bai, R. Sun, Z. Wang, H. Jang, F. Zhang, Y. Ma, Z. Xu, X. Feng, T. Xie, Y. Huang, Y. Zhang, J.A. Rogers, Freestanding 3D mesostructures, functional devices, and shape-programmable systems based on mechanically induced assembly with shape memory polymers. *Adv. Mater.* **31**, 1805615 (2019).
30. A.S. Gladman, E.A. Matsumoto, R.G. Nuzzo, L. Mahadevan, J.A. Lewis, Biomimetic 4D printing. *Nat. Mater.* **15**, 413 (2016).
31. A. Kotikian1, C. McMahan, E.C. Davidson, J.M. Muhammad, R.D. Weeks, C. Daraio, J.A. Lewi, Untethered soft robotic matter with passive control of shape morphing and propulsion. *Sci. Robotics* **4**, eaax7044 (2019).
32. X. Liao, J. Xiao, Y. Ni, C. Li, X. Chen, Self-assembly of islands on spherical substrates by surface instability. *ACS Nano* **11**, 2611 (2017).
33. J.W. Boley, W.M. van Rees, C. Lissandrello, M.N. Horenstein, R.L. Truby, A. Kotikian, J.A. Lewis, L. Mahadevan, Shape-shifting structured lattices via multimaterial 4D printing. *Proc. Natl. Acad. Sci. U.S.A.* **116**, 20856 (2019).
34. S. Xu, Z. Yan, K.I. Jang, W. Huang, H. Fu, J. Kim, Z. Wei, M. Flavin, J. McCracken, R. Wang, A. Badea, Y. Liu, D. Xiao, G. Zhou, J. Lee, H.U. Chung, H. Cheng, W. Ren, A. Banks, X. Li, U. Paik, R.G. Nuzzo, Y. Huang, Y. Zhang, J.A. Rogers, Assembly of micro/nanomaterials into complex, three-dimensional architectures by compressive buckling. *Science* **347**, 154 (2015).
35. Y. Zhang, F. Zhang, Z. Yan, Q. Ma, X. Li, Y. Huang, J.A. Rogers, Printing, folding and assembly methods for forming 3d mesostructures in advanced materials. *Nat. Rev. Mater.* **2**, 17019 (2017).
36. X. Ning, H. Wang, X. Yu, J. Soares, Z. Yan, K. Nan, G. Velarde, Y. Xue, R. Sun, Q. Dong, H. Luan, C.M. Lee, A. Chempakasseril, M. Han, Y. Wang, L. Li, Y. Huang, Y. Zhang, J.A. Rogers, Three-dimensional multiscale, multistable, and geometrically diverse microstructures with tunable vibrational dynamics assembled by compressive buckling. *Adv. Funct. Mater.* **27**, 1605914 (2017).
37. H. Wang, X. Ning, H. Li, H. Luan, Y. Xue, X. Yu, Z. Fan, L. Li, J.A. Rogers, Y. Zhang, Y. Huang, Vibration of mechanically-assembled 3D microstructures formed by compressive buckling. *J. Mech. Phys. Solids* **112**, 187 (2018).
38. H. Li, X. Wang, F. Zhu, X. Ning, H. Wang, J.A. Rogers, Y. Zhang, Y. Huang, Viscoelastic characteristics of mechanically assembled three-dimensional structures formed by compressive buckling. *J. Appl. Mech.* **85**, 121002 (2018).
39. W. Kreider, A.H. Nayfeh, Experimental investigation of single-mode responses in a fixed-fixed buckled beam. *Nonlinear Dynamics* **15**, 155 (1998).
40. G.B. Min, J.G. Eisley, Nonlinear vibration of buckled beams. *J. Eng. Ind.* **94**, 637 (1972).
41. X. Ning, X. Yu, H. Wang, R. Sun, R.E. Corman, H. Li, C.M. Lee, Y. Xue, A. Chempakasseril, Y. Yao, Z. Zhang, H. Luan, Z. Wang, W. Xia, X. Feng, R.H. Ewoldt, Y. Huang, Y. Zhang, J.A. Rogers, Mechanically active materials in three-dimensional mesostructures. *Sci. Adv.* **4**, eaat8313 (2018).
42. K.I. Jang, K. Li, H.U. Chung, S. Xu, H.N. Jung, Y. Yang, J.W. Kwak, H.H. Jung, J. Song, C. Yang, A. Wang, Z. Liu, J.Y. Lee, B.H. Kim, J.H. Kim, J. Lee, Y. Yu, J. Bu Kim, H. Jang, K.J. Yu, J. Kim, J.W. Lee, J.W. Jeong, Y.M. Song, Y. Huang, Y. Zhang, J.A. Rogers, Self-assembled three dimensional network designs for soft electronics. *Nat. Commun.* **8**, 1 (2017).
43. F. Zhang, F. Liu, Y. Zhang, Analyses of mechanically-assembled 3D spiral mesostructures with applications as tunable inductors. *Science China Technological Sciences* **62**, 243 (2019).
44. B.H. Kim, F. Liu, Y. Yu, H. Jang, Z. Xie, K. Li, J. Lee, J.Y. Jeong, A. Ryu, Y. Lee, D.H. Kim, X. Wang, K. Lee, J.Y. Lee, S.M. Won, N. Oh, J. Kim, J.Y. Kim, S.J. Jeong, K.I. Jang, S. Lee, Y. Huang, Y. Zhang, J.A. Rogers, Mechanically guided post-assembly of 3D electronic systems. *Adv. Funct. Mater.* **28**, 1803149 (2018).
45. Z. Yan, M. Han, Y. Shi, A. Badea, Y. Yang, A. Kulkarni, E. Hanson, M.E. Kandel, X. Wen, F. Zhang, Y. Luo, Q. Lin, H. Zhang, X. Guo, Y. Huang, K. Nan, S. Jia, A.W. Oraham, M.B. Mevis, J. Lim, X. Guo, M. Gao, W. Ryu, K.J. Yu, B.G. Nicolau, A. Petronico, S.S. Rubakhin, J. Lou, P.M. Ajayan, K. Thornton, G. Popescu, D. Fang, J.V. Sweedler, P.V. Braun, H. Zhang, R.G. Nuzzo, Y. Huang, Y. Zhang, J.A. Rogers, Three-dimensional mesostructures as high-temperature growth templates, electronic cellular scaffolds, and self-propelled microrobots. *Proc. Natl. Acad. Sci. U.S.A.* **114**, E9455 (2017).
46. K. Nan, S.D. Kang, K. Li, K.J. Yu, F. Zhu, J. Wang, A.C. Dunn, C. Zhou, Z. Xie, M.T. Agne, H. Wang, H. Luan, Y. Zhang, Y. Huang, G.J. Snyder, J.A. Rogers, Compliant and stretchable thermoelectric coils for energy harvesting in miniature flexible devices. *Sci. Adv.* **4**, Eaau5849 (2018).
47. S.M. Won, H. Wang, B.H. Kim, K. Lee, H. Jang, K. Kwon, M. Han, K.E. Crawford, H. Li, Y. Lee, Y. Lee, X. Yuan, S.B. Kim, Y.S. Oh, W.J. Jang, J.Y. Lee, S. Han, J. Kim, X. Wang, Z. Xie, Y. Zhang, Y. Huang, J.A. Rogers, Multimodal sensing with a three-dimensional piezoresistive structure. *ACS Nano* **13**, 10972 (2019).
48. X. Ning, X. Wang, Y. Zhang, X. Yu, D. Choi, N. Zheng, D.S. Kim, Y. Huang, Y. Zhang, J.A. Rogers, Assembly of advanced materials into 3D functional structures by methods inspired by origami and kirigami: a review. *Adv. Mater. Interfaces* **5**, 1800284 (2018).
49. X. Guo, Z. Xu, F. Zhang, X. Wang, Y. Zi, J.A. Rogers, Y. Huang, Y. Zhang, Reprogrammable 3D mesostructures through compressive buckling of thin films with prestrained shape memory polymer. *Acta Mechanica Solida Sinica* **31**, 589 (2018).
50. K. Li, W. Wu, Z. Jiang, S. Cai, Voltage-induced wrinkling in a constrained annular dielectric elastomer film. *J. Appl. Mech.* **85**, 011007 (2018).
51. G. Mao, L. Wu, X. Liang, S. Qu, Morphology of voltage-triggered ordered wrinkles of a dielectric elastomer sheet. *J. Appl. Mech.* **84**, 111005 (2017).

52. M. Han, H. Wang, Y. Yang, C. Liang, W. Bai, Z. Yan, H. Li, Y. Xue, X. Wang, B. Akar, H. Zhao, H. Luan, J. Lim, I. Kandela, G.A. Ameer, Y. Zhang, Y. Huang, J.A. Rogers, Three-dimensional piezoelectric polymer microsystems for vibrational energy harvesting, robotic interfaces and biomedical implants. *Nat. Electronics* **2**, 26 (2019).
53. S. Li, M. Han, J.A. Rogers, Y. Zhang, Y. Huang, H. Wang, Mechanics of buckled serpentine structures formed via mechanics-guided, deterministic three-dimensional assembly. *J. Mech. Phys. Solids* **125**, 736 (2019).
54. J. Ren, S. Yu, N. Gao, Q. Zou, Indentation quantification for in-liquid nanomechanical measurement of soft material using an atomic force microscope: Rate-dependent elastic modulus of live cells. *Phys. Rev. E* **88**, 5 (2013).
55. K. Nan, H. Wang, X. Ning, K.A. Miller, C. Wei, Y. Liu, H. Li, Y. Xue, Z. Xie, H. Luan, Y. Zhang, Y. Huang, J.A. Rogers, P.V. Braun, Soft three-dimensional microscale vibratory platforms for characterization of nano-thin polymer films. *ACS Nano* **13**, 449 (2018).
56. E. Karzbrun, A. Kshirsagar, S.R. Cohen, J.H. Hanna, O. Reiner, Human brain organoids on a chip reveal the physics of folding. *Nat. Phys.* **14**, 515 (2018).
57. H. Clevers, Modeling development and disease with organoids. *Cell* **165**, 1586 (2016).
58. A. Bhaduri, M.G. Andrews, W.M. Leon, D. Jung, D. Shin, D. Allen, D. Jung, G. Schmunk, M. Haeussler, J. Salma, A.A. Pollen, T.J. Nowakowski, A.R. Kriegstein, Cell stress in cortical organoids impairs molecular subtype specification. *Nature* **578**, 142 (2020).
59. N. Sachs, A. Papaspyropoulos, D.D. Zomer-van Ommen, I. Heo, L. Böttinger, D. Klay, F. Weeber, G. Huelsz-Prince, N. Iakobachvili, G.D. Amatngalim, J. Ligt, A. Hoeck, N. Proost, M.C. Viveen, A. Lyubimova, L. Teeven, S. Derakhshan, J. Korving, H. Begthel, J.F. Dekkers, K. Kumawat, E. Ramos, M.FM. Oosterhout, G.J. Offerhaus, D.J. Wiener, E.P. Olimpio, K.K. Dijkstra, E.F. Smit, M. Linden, S. Jaksani, M. Ven, J. Jonkers, A.C. Rios, E.E. Voest, C.HM. Moorsel, C.K. Ent, E. Cuppen, A. Oudenaarden, F.E. Coenjaerts, L. Meyaard, L.J. Bont, P.J. Peters, S.J. Tans, J.S. Zon, S.F. Boj, R.G. Vries, J.M. Beekman, H. Clevers, Long-term expanding human airway organoids for disease modeling. *The EMBO Journal* **38**, e100300 (2019).
60. C.F. Guimarães, L. Gasperini, A.P. Marques, R.L. Reis, The stiffness of living tissues and its implications for tissue engineering. *Nat. Rev. Mater.* **5**, 351 (2020).
61. H. Hu, H. Gehart, B. Artegiani, C. Löpez-Iglesias, F. Dekkers, O. Basak, J.v. Es, S.M.C.d.S. Lopes, H. Begthel, J. Korving, M.v.d. Born, C. Zou, C. Quirk, L. Chiriboga, C.M Rice, S. Ma, A. Rios, P.J. Peters, Y.P.d. Jong, H. Clevers, Long-term expansion of functional mouse and human hepatocytes as 3D organoids. *Cell* **175**, 6 (2018).
62. K. Ronaldson-Bouchard, S.P. Ma, K. Yeager, T. Chen, L. Song, D. Sirabella, K. Morikawa, D. Teles, M. Yazawa, G. Vunjak-Novakovic, Advanced maturation of human cardiac tissue grown from pluripotent stem cells. *Nature* **556**, 7700 (2018).
63. A. Rigato, A. Miyagi, S. Scheuring, F. Rico, High-frequency microrheology reveals cytoskeleton dynamics in living cells. *Nat. Phys.* **13**, 8 (2017).